Estimation of the time, location and natural frequency of entrained bubbles, through identification of individual bubble signatures in a severely overlapping, noisy surf zone environment

G. T. Yim, P. R. White, T. G. Leighton

Institute of Sound and Vibration Research, University of Southampton, Highfield, Southampton, SO17 1BJ, UK. gty@isvr.soton.ac.uk, prw@isvr.soton.ac.uk, tgl@isvr.soton.ac.uk

Abstract

This paper describes how the Gabor transform can assist in the identification of the acoustic signatures, emitted by individual ringing bubbles when for example entrained by a breaking wave, under conditions where noise and the degree of overlap between these signatures hinders such identification. Once identified, the natural frequencies of the individual bubbles, and the moment they begin ringing, can be determined. In addition, if an array of hydrophones is used, the location of each bubble can be estimated. However whilst the use of the Gabor transform may be necessary in the surf zone, where the noise and overlap problems are severe, its inclusion in the signal processing compromises the spatial and temporal resolution of the estimates. Hence an additional stage is introduced, whereby the Gabor technique is initially applied to identify the individual bubble signatures in hydrophone records of surf zone ambient noise, and then is removed to obtained increased resolution from analysis of the signal in that region of the time history and time-frequency domain in which the Gabor technique has localised a potential signature. This allows the times of entrainment, the locations, and the natural frequencies of individual bubbles to be identified during wave breaking events in the surf zone.

1. Introduction

If a bubble emits, on entrainment, a passive emission which is detected by the hydrophones of an appropriate array, it is in principle a straightforward matter to identify the natural frequency of that bubble, and to estimate the location of the source and time at which it began to emit. This is not a simple matter, however, if the signals are noisy and the emissions overlap in time, as can be the case in the surf zone. This paper makes use of the Gabor transform to identify potential bubble emissions in the time-frequency domain. However there are two further issues which need to be addressed. First, in producing a time-frequency plot of the Gabor coefficients, resolution in time and frequency are compromised to such a degree that, for example, estimation of the location of the emitting bubble is extremely poor (of order 12 m). Second, whilst the Gabor transform preferentially identified exponentially decaying sinusoids of the type emitted by entrained bubbles, there is still a chance that a peak in the plot of the Gabor coefficient might be the result of noise spikes in the time-frequency plot. Correlation of peaks in the Gabor coefficient plots (and source time series) from all the available hydrophones in the array reduces that risk, although localised sources of exponentially decaying sinusoids (such as could conceivably be caused by impact against the rig) might still be identified as bubbles. Hence the final stage of processing allows identification of those noise sources which are located away from rig structures, and hence are not self-noise.

Wavebreaking in the surf zone is one of the wide range of physical mechanisms that can give rise to bubble generation. Bubbles may be entrained at a liquid surface or through the comminution of existing bubbles. A significant proportion of the energy generated in these processes is radiated as acoustic energy. Within the free-field approximation, for air bubbles in water of sizes greater than a few tens of microns, the frequency of oscillation of a bubble is inversely proportional to it size [1]. Thus monitoring of the acoustic emissions at bubble formation allows one, in principle, to measure the size of the bubble formed. For small amplitudes of oscillation the bubble motion can be approximated by a lightly damped second order linear differential equation [2], the impulse response of which is an exponentially damped sinusoid [3, 4]. The principle of detecting and characterising these emissions has been used to estimate bubble size distributions in the natural [5]. Furthermore, the emissions from bubbles during entrainment have been studied in a variety of scenarios, including bubble clouds formed during injection [6], the impact of bodies of water [7, 8] and liquid jets [9, 10]. Additional work has considered the bubble signatures generated when a liquid drop impacts with a surface including rainfall [11] and wavebreaking [12].

In carefully controlled conditions, where signal to noise ratios are high and bubble entrainment rates are low, then the task of isolating individual bubble signatures is relatively straightforward. In practical measurement scenarios one is often faced with adverse signal to noise ratios and rapid entrainment rates, so that bubble

signatures overlap, with multiple bubble signatures occurring simultaneously and many bubbles occupying the same frequency band. One approach to estimating the bubble size distribution is to compute the power spectral density (by time-averaging Fourier transform of finite data lengths) and then employ inverse techniques to infer the bubble size distribution that gave rise to that spectrum [13]. Such an approach results in loss temporal information, and hence in precise localisation by triangulation of the sound source, which is one objective of this work.

Leighton *et al.* [14, 15] provided an alternative method, which retained temporal information in overlapping, noisy environments. They exploited the Gabor transform to identify the individual bubble signatures in a test tank under a plunging jet and a waterfall [15], and in the ocean during rainfall [14]. They used this data to test a theory for bubble fragmentation [16]. In this paper this technique is applied to ambient noise gathered in the surf zone during the Hurst Spit experiment in 2000 [17], to obtain the times of entrainment, the locations, and the natural frequencies of individual bubbles under breaking waves in the surf zone.

2. Method

2.1 Apparatus

A detailed discussion of the experimental configuration can be found in a companion paper in this volume [17]. This experiment exploited an array of four sensors. Originally the array consisted of eleven elements, but at the time of data collection only four were functioning. Crucially, the out-of-plane hydrophone had been damaged by the extreme conditions in the surf, and hence the results of the triangulation contain a left-right ambiguity. The configuration of the surviving sensors is shown in Figure 1.
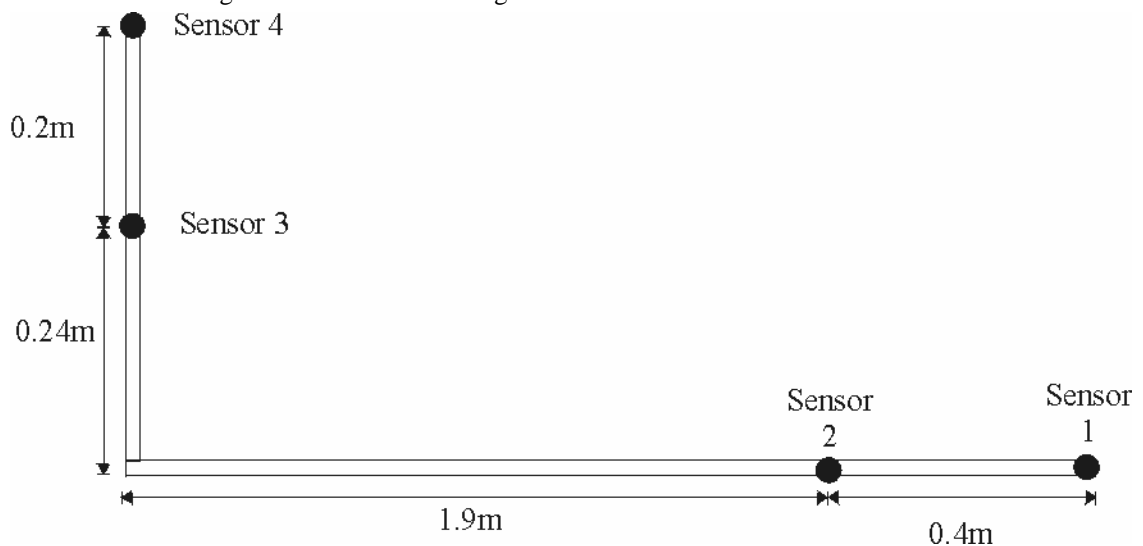
Figure 1. Side view of the array geometry. All the surviving hydrophones lay in a plane, the normal to which was horizontal. The vertical line drawn in the figure, joining sensors 3 and 4, would be vertical in situ, and is at the end of the array furthest from the shore. The horizontal line running from sensor 2 to 1 would run towards the shore, and would be horizontal in situ.

2.2 Signal processing

The goal of the signal processing is first to isolate individual bubble signatures, second to estimate the relative delays between the hydrophone channels, and finally to estimate the source location from the delays (triangulation). Each of these tasks will be addressed individually in the following sub-sections.

2.2.1 Signal Localisation

The objective is to detect the presence of a bubble signature. If the entrainment rate is high these signatures may overlap in time, in which case simple energy-based detectors will fail to separate the two bubble signatures. However a time-frequency based detector allows signature separation in such a scenario (assuming the two bubbles have different natural frequencies).

There are many time-frequency methods that could be adopted [18]. The general class of bilinear representations suffers from problems associated with cross-terms, a problem that becomes more critical at low SNRs. The spectrogram [18] offers a simple, efficient, algorithm based on the FFT in which the cross-terms have limited impact. Potentially the data files to be processed are large and one seeks to minimise redundancy in the

time-frequency representation. This naturally leads one to consider orthonormal representations, in which there is no redundancy: N input samples in the time series generates N points in the time-frequency plane. The first time-frequency method used for detection falls into this category and can be expressed as:

$$S(m,k) = \left| \sum_{m=0}^{L-1} x(n-mL) e^{-2\pi i n k / L} \right|^2 \tag{1}$$

This is a spectrogram that is computed using a rectangular window with no overlapping. The window length L is selected by the user. Short windows yield poor frequency resolution, whilst longer windows yield poor temporal resolution. The step size is m, and k is the discrete frequency index.

This spectrogram can be considered as decomposing a signal into components that are rectangular sinusoidal pulses. These basis functions only match the bubble signatures over short a duration (when the amplitude can be considered as approximately constant). A basis set that is better matched to the bubble signature is provided by exponentially windowed sinusoids. To employ such a basis set one has to resort to using a bi-orthogonal basis. Such bases require two windows: one to perform the signal decomposition, and the second to perform the signal reconstruction. A scheme to perform such a decomposition was presented by Friedlander and Porat [19]. This is an efficient algorithm, exploiting the computational efficiency of the FFT. This algorithm can be viewed as a spectrogram, with a suitable windowing function. However in this paper we shall refer to this transform as the exponential Gabor transform (or simply the 'Gabor' transform) in order to distinguish it from the above spectrogram.

By way of illustration, compare the spectrogram and Gabor representations of simple signal consisting of three decaying, overlapping exponentials, shown in Figure 2. Figure 2a shows the time series in which the three exponential components can be seen. Figure 2b shows a plot displaying the magnitude of the Gabor representation of this signal. There are only three non-zero values in this discrete plot, one representing each of the components. Compare this with the spectrogram shown in Figure 2c, where each of the components generates a range of non-zero terms. This smearing results in a loss of energy in the peak value. How this can make the Gabor transform more robust to the presence of noise and overlap in the detection of bubble entrainment signatures is described by Leighton *et al.* [15].
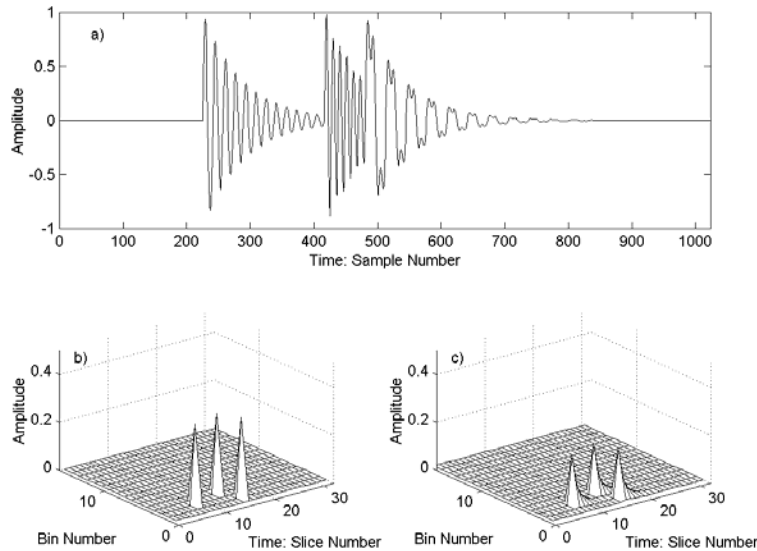
Figure 2. Decomposition of Synthetic Signal. (a) Synthesized time series data (representing, for example, the output of a hydrophone) consisting of a summation of three exponentially decaying sinusoids; (b) Time-frequency representation of the amplitude of the Gabor coefficients when the time-series of part 'a' is processed using the Gabor transform; (c) Spectrogram of the data from part 'a'. Plots 'b' and 'c' are normalised so that the total volume under the curves is unity. This is the simplest level of illustration. For example the start times and centre frequencies of the exponential terms are especially chosen so that minimal leakage occurs for 'b' and 'c.

In general the fact that the Gabor transform is better matched to the signal model means that this leakage will, on average, be small than that encountered by the spectrogram. Hence throughout the following the Gabor transform will be used to compute the time frequency plots, this choice being based on the observation that the

bubble signatures more closely resemble decaying exponentials than constant amplitude sinusoids.

An example of the time history obtained in the surf zone by a hydrophone in the Hurst Spit 2000 trial is shown in Figure 3. The identification of individual bubble signatures is not a simple as was the case in Figure 2a.
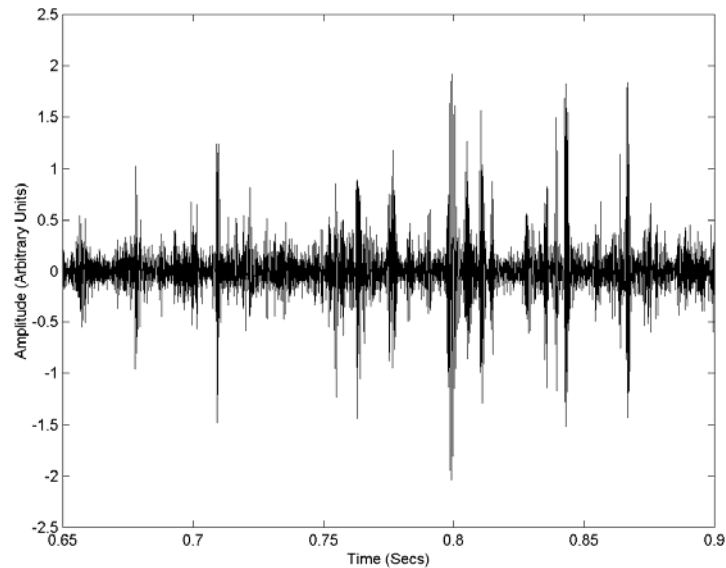
Figure 3. A section of time series data obtained by a hydrophone in the Hurst Spit 2000 surf zone trial. The time axis matches that used in Figure 4. Environmental data: Time=10.59; Date=10 November 2000; Wind Speed=8 mph; Wind Direction=SW; Water temperature=12°C; Air temperature=12°C; Water depth=approx. 1m; Notes: Calm sea.

The procedure adopted when isolating bubble signatures from such time histories is to compute the Gabor transform, although our associated tests suggest that use of the spectrogram would result in only a small loss of performance. An example result is shown in Figure 4.
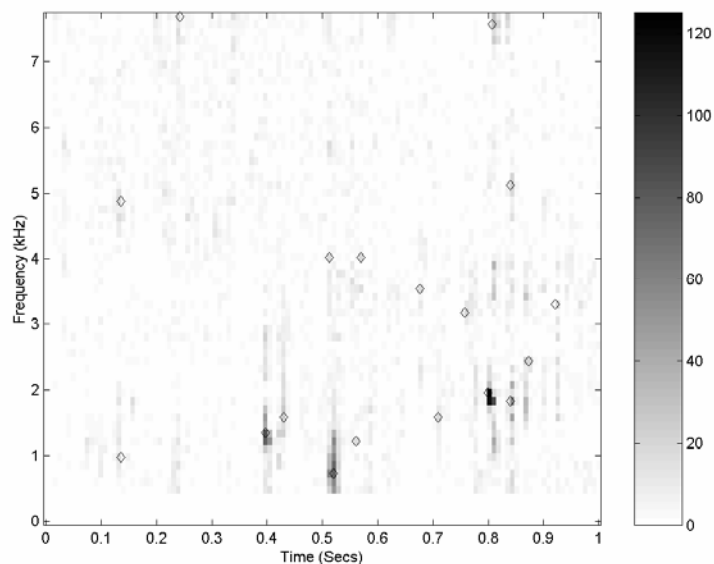
Figure 4. Normalised Gabor representation of a hydrophone signal, a section of which was shown in Figure 3. The detection threshold was set equal to 15 units (normalised amplitude, shown in grey scale). The diamonds mark events above the detection threshold, which are flagged for subsequent testing to determine whether they are bubble signatures.

It should be emphasised that no filter is applied to the presentation of the data. A detection threshold is applied, however, to identify the peaks which are candidates, subject to further checks, for identification as

bubble signatures. A frequency dependent detection threshold, $T(k)$, is used to account for the coloration of the ambient noise field. This threshold is computed using:

$$T(k) = C\, median\{|G(n,k)|^2\} \tag{2}$$

where $G(n,k)$ is the Gabor transform and *median{•}* denotes the operation of taking the median of the data (over the time variable n) and C is a user defined constant. The use of the median allows one to estimate the background noise spectrum even in the presence of transient signals [20]. The selection of the parameter C allows one to reduce the number of false alarms at the expense of reduced sensitivity. In practice this threshold is set at a relatively large level so that the system is not overwhelmed with spurious detections. This frequency dependent threshold can be alternatively implemented using a fixed threshold and the following normalised distribution, $\widetilde{G}(n,k)$ defined as:

$$\widetilde{G}(n,k) = \frac{|G(n,k)|^2}{median\{|G(n,k)|^2\}} \tag{3}$$

Figure 4 shows the normalised Gabor transform for a real data set, plotted as a grey scale image (using the conventional of large values being represented by dark shades of grey). As we have seen each signature can give rise to several large coefficients in the Gabor transform (and in the spectrogram). These coefficients are clustered close to the maximum. In order to avoid one signature giving rise to several detections, a small region around each peak is declared as void and no other detections in this region are counted (6dB points: 18 ms, 180 Hz). If these detections occur in sufficient of the channels, at similar times and frequencies, then a bubble signature is said to have been isolated.

2.2.2 Estimation of Relative Delays

The time-frequency representations are computed every L samples, where L is the window size and is typically of the order of *100*. This loss in temporal resolution means that the time-frequency plots cannot be used to estimate the delays between hydrophone signals. For example, the finite time increments of the Gabor transform would allow the acoustic path length to be resolved to no better than 12 m in any single hydrophone trace. Therefore the procedure used here is to take the original time series in vicinity of each peak, for each channel. One channel is selected as the reference channel and the relative delay for all the other channels are computed use cross-correlation. The cross-correlation is not affected by overlapping signatures, assuming that the bandwidths of the two signatures do not overlap.

The use of cross-correlation for delay estimation is nearly optimal for uncorrelated noise environments and optimal schemes can be implemented under these assumptions [21]. We chose to incur, at worst, a small reduction in performance in favour of the simplicity of a cross-correlation scheme. Additionally one cannot easily implement optimal schemes in spatially correlated noise, such as that encountered in the ocean, unless the character of the noise can be estimated separately.

2.2.3 Source Localisation

Once all the relative delays between sensors have been estimated, the task remains of converting these delays into a source position, within the 3-D space surrounding the array. Note that in our experimental configuration four sensors were available, from which six unique relative delays can be computed. Seven hydrophones, including the out-of-plane hydrophone, were damaged by the extreme conditions encountered on site (with sustained windspeeds of in excess of 50 mph) [17]. The only four functioning sensors for the ambient noise tests lay within a plane. This led to an inherent positioning ambiguity, such that it is impossible to determine which side of the plane a source was located.

This source localisation assumes a homogeneous medium, such that the acoustic rays travel in straight lines and so the delay between the mth and n^{th} sensor, $\tau_{m,n}$, is given by:

$$\tau_{m,n} = c\, d_{m,n} \tag{3}$$

where $d_{m,n}$ is the path difference between the two sensors and c is the speed of propagation (assumed to be constant). The source location is based on a least squares optimisation, specifically the following cost function is minimised:

$$\Psi(\underline{r}) = \sum_m \sum_{n,\, n \leq m} \left(d_{m,n} - \hat{d}_{m,n}\right)^2 \tag{4}$$

where $d_{m,n}$ is the theoretical path difference based on an source position vector $\underline{r}=(x,y,z)$, whilst $\hat{d}_{m,n}$ are the path

differences measured from the data. It can readily be shown that the function Ψ is a non-linear function data that cannot be analytically minimised. This error surface may contain local minima. The approach adopted here to the minimisation of Ψ is a two-stage strategy where initially a relatively coarse grid of candidate positions, <u>r</u>, are considered. The point on this grid that minimises the cost function is taken as the starting position for a Nelder-Meade optimisation scheme [22].

3. Results

The methods described in Section 2 where applied to data gathered from the Hurst Spit 2000 experiment. Figure 5 shows all for the bubbles emitting within a cube of seawater 20 cm on a side, as determined from a 1 s record of the four hydrophones. The frequency band considered was limited to 0.5-8kHz (though surprisingly all the bubbles detected were in the band 1.5-2.3 kHz). At the location of the sound source, a symbol is placed which indicates the frequency band in which it emits (animations are available which, at the time each source begins to emit, both plots its location and plays the commensurate natural frequency).
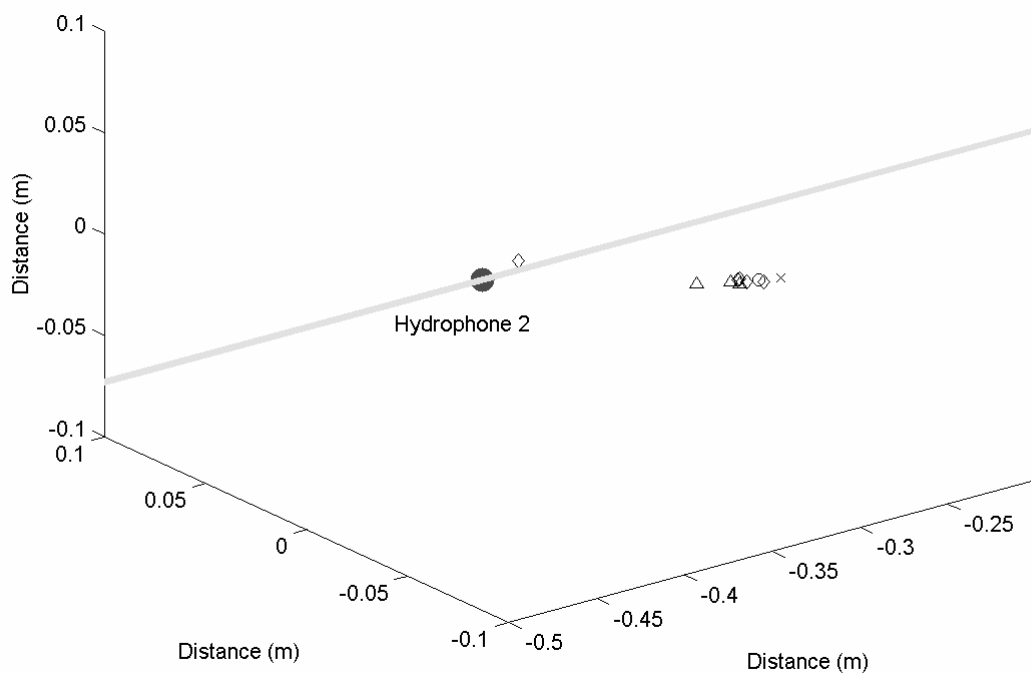
Figure 5. The locations and natural frequencies of the bubbles which, during a particular second of data, emit 'signatures' within a cube of seawater which measures 20 cm on a side. One face of this cube contains a hydrophone from the horizontal array, as marked by the dark circle. The grey line running through hydrophone 2 marks the horizontal, and passes through the hydrophones in the horizontal array (see Figure 1). It points out to sea at its left extremity (where it intersects the vertical axis), and points towards shore at it right extremity. As the intersection shows, the base of the cube is 2.5 cm below the level of the hydrophone. The points show the locations of 'ringing' bubbles, with the symbol indicating the natural frequency: circles=1.5-1.7 kHz; diamonds=1.7-1.9 kHz; triangles=1.9-2.1 kHz; crosses=2.1-2.3 kHz.

4. Conclusions

From Figure 5 it is possible to make certain observations about the natural frequencies and locations of the entrained bubbles (the accompanying animation also indicates the timing of their emissions). Objective (iii) from section 3 of Leighton *et al.* [17] has been accomplished. For the example shown in Figure 5, despite the frequency band of 0.5-8 kHz made available to the search, the bubbles all have natural frequencies in a narrow band, 1.5-2.3 kHz. Furthermore, the bulk of the 8 litre volume investigates is empty of 'ringing' bubbles (though presumably contains many silent ones): the emitting bubbles all occur in a tight cluster, suggesting a localised entrainment for fragmentation event. It should be remembered that this paper represents the first stages in a fuller study of entrainment emissions [17], and hence it is wise to treat these findings as preliminary results. The limitations should be borne in mind. Some, such as the left-right ambiguity, are not fundamental but simply accidents of the field trial, which with luck should not trouble future work. Others are more fundamental. These include as the fact that any source of an exponentially decaying sinusoid (e.g. the possible impact of gravel against the scaffolding of

the rig) will also be identified as bubbles, unless the ability to localise the source of the emission is used to eliminate such features from the findings. The ability to precisely locate the source will also allow identification of the extent to which a rig will itself entrain bubbles.

Acknowledgements

References

[1]   Minnaert M. On musical air-bubbles and sounds of running water. *Phil. Mag.* 1933; **16**: 235-248.

[2]   Devin C. Survey of thermal, radiation and viscous damping of pulsating air bubbles in water. *J. Acoust. Soc. Am.* 1959; **31**: 1654-1667.

[3]   Strasberg M. The pulsation frequency of nonspherical bubbles. *J.Acoust.Soc.Am.* 1953; **25**: 536-537.

[4]   Strasberg M. Gas bubbles as sources of sound in water. *J. Acoust. Soc. Am.* 1956; **28**: 20-26.

[5]   Leighton TG and Walton AJ. An experimental study of the sound emitted from gas bubbles in a liquid. *Eur. J. Phys.* 1987; **8**: 98-104.

[6]   Nicholas M, Roy RA, Crum LA, Oguz HN and Prosperetti A. Sound emissions by a laboratory bubble cloud. *J. Acoust. Soc. Am.,* 1994; **94**: 3171-3182.

[7]   Kolaini AR, Roy RA and Crum LA. An investigation of the acoustic emissions from a bubble plume. *J. Acoust. Soc. Am.* 1991; **89**: 2452-2455.

[8]   Oguz HN, Prosperetti A and Kolaini AR. Air entrapment by a falling water mass. *J. Fluid Mech.,* 1995; **294**: 181-207.

[9]   Hwang PA, Yu YK and Wu J. Temperature effects on generation and entrainment of bubbles induced by a water jet. *J. Physical Oceanog.*, 1991; **21**: 1602-1605.

[10]   Prosperetti A and Oguz HN. Air entrainment upon liquid impact. *Phil. Trans. Roy. Soc. Lond.,* 1997; **355**: 491-506.

[11]   Pumphrey HC, Crum LA and L. Bjørnø L. Underwater sound produced by individual drop impacts and rainfall. *J. Acoust Soc Am,* 1989; **85**: 1518-1526.

[12]   Medwin H and Beaky MW. Bubble sources of the Knudsen sea noise spectra. *J. Acoust Soc Am*, 1989; **86**: 1124-1130.

[13]   Loewen MR and Melville WK. A model for the sound generated by breaking waves. *J. Acoust Soc Am*, 1991; **90**: 2075-2080.

[14]   Leighton TG, Schneider MF and White PR. Study of dimensions of bubble fragmentation using optical and acoustic techniques, in *Proceedings of the third International Meeting on Natural Physical Processes Related to Sea Surface Sound*. M J Buckingham and J Potter (eds.), World Scientific Publishing Ltd., Singapore, 1995 pp. 414-428

[15]   Leighton TG, White PR and Schneider MF. The detection and dimension of bubble entrainment and comminution. *J. Acoust Soc Am*, 1998; **103**: 1825-1835.

[16]   Longuet-Higgins MS. The crushing of air cavities in a liquid. *Proc. R. Soc. Lond.* 1992; **439**: 611-626.

[17]   Leighton TG, Meers SD, Simpson MD, Clarke JWL, Yim GT, Birkin PR, Watson Y, White PR, Heald GJ, Dumbrell HA, Culver RL and Richards SD. The Hurst Spit experiment: The characterisation of bubbles in the surf zone using multiple acoustic techniques, in *'Acoustical Oceanography', Proceedings of the Institute of Acoustics Vol. 23 Part 2, 2001*, T G Leighton, G J Heald , H Griffiths and G Griffiths, (eds.), Institute of Acoustics, (this volume).

[18]   Cohen L. Time-Frequency Analysis. Prentice-Hall, 1995.

[19]   Friedlander B and B. Porat B. Detection of Transient Signals by the Gabor Representation. *IEEE Trans. Acoust., Speech, Signal Processing* 1989; **37**: 169-180.

[20]   Leung TS-T and White PR. Robust Estimation of Oceanic Background Spectrum, in *Mathematics in Signal Processing IV*, J G McWhirter and I K Proudler eds. (Clarendon Press, Oxford), 1998, pp. 369-382.

[21]   Carter GC and Robinson ER. Ocean Effects on Time Delay Estimation Requiring Adaptation. *IEEE J. of Oceanic Engineering*, 1993; **18**: 367-378.

[22]   Press W, Vetterling W, Teukolsky S and Flannery B. Numerical Recipes in C – The Art of Scientific Computing. Cambridge University Press, Cambridge, 1992.